New Journal of Physics
The open access journal at the forefront of physics

Deutsche Physikalische Gesellschaft DPG IOP Institute of Physics

PAPER • OPEN ACCESS

Quantum information processing using frozen core Y^{3+} spins in Eu^{3+}:Y_2SiO_5

To cite this article: Manjin Zhong *et al* 2019 *New J. Phys.* **21** 033019

New Journal of Physics
The open access journal at the forefront of physics

Deutsche Physikalische Gesellschaft DPG
IOP Institute of Physics

Published in partnership with: Deutsche Physikalische Gesellschaft and the Institute of Physics

OPEN ACCESS

RECEIVED
13 December 2018

REVISED
15 February 2019

ACCEPTED FOR PUBLICATION
5 March 2019

PUBLISHED
28 March 2019

PAPER

Quantum information processing using frozen core Y^{3+} spins in Eu^{3+}:Y_2SiO_5

Manjin Zhong[1,3], **Rose L Ahlefeldt**[2] **and Matthew J Sellars**[2]

[1] Shenzhen Institute for Quantum Science and Engineering, and Department of Physics, Southern University of Science and Technology, Shenzhen 518055, People's Republic of China
[2] Centre for Quantum Computation and Communication Technology, Research School of Physics and Engineering, The Australian National University, Canberra 0200, Australia
[3] Author to whom any correspondence should be addressed.

E-mail: zhongmj@sustech.edu.cn

Keywords: quantum information, quantum memory, rare earth, entanglement, solid state spectroscopy, spin dynamics

Abstract

In this paper, we present a method to investigate and control the dynamics of the nearby host nuclear spins (the 'frozen core') about a rare-earth ion doped in a crystal. Optically detected, double quantum magnetic resonance measurements were conducted on Eu^{3+}: Y_2SiO_5. The distinct magnetic resonant frequencies of nearby Y^{3+} spins were measured along with the lifetime and coherence time of an individual Y^{3+} spin. We demonstrate an entangling gate between the Eu^{3+} spins and a Y^{3+} spin associated with a particular position. Further, we propose a method to initialize the Y^{3+} spin states, enabling the Y^{3+} spins to be used as a quantum resource for quantum information applications.

1. Introduction

Rare-earth solids have been identified as promising candidates for quantum memories in a series of recent demonstrations, including storage of quantum states with high efficiency [1–3] and long storage times [4–6], multimode storage [6–8] and entanglement storage [9, 10]. In part, the interest in using rare earths for quantum memories is due to the long quantum coherence times observed for both optical and spin transitions in these systems [11–19].

A major issue for these rare-earth based memories is that no crystal hosts have been identified which are nuclear-spin-free and at the same time have the high solubility of rare-earth ions required for the memory applications. As a result, the interaction of the rare-earth ions with the unavoidable nuclear spin bath continues to be a significant issue in maximizing the quantum coherence times and hence storage time of these systems. Having said this, long coherence times on both optical and spin transitions have been observed, which were achieved by applying techniques to decouple the rare-earth ions from the bath [13, 14, 17–20]. The first technique commonly used is working at zero first order Zeeman (ZEFOZ) points: magnetic fields at which the transition has zero gradient in frequency with field and so is first-order insensitive to magnetic field fluctuations [13]. At a ZEFOZ point, dynamic decoherence control (DDC) [21, 22] is often employed to actively rephase any decoherence slower than the applied control sequence. These techniques are very successful: some of the longest coherence times ever observed in solid-state systems have been observed on hyperfine transitions of rare-earth ions in crystals that have a high density of nuclear spins. However, even in those measurements the residual interactions with the spin bath limited the observed coherence times. Improvements in the decoupling techniques could lead to further extension of these times.

The decoupling techniques that have so far been employed on the rare-earth systems are relatively generic; their design is based on the premise that the effect of the bath can be treated as a simple perturbative field acting on the rare-earth ion. They do not take into account the details of the interactions of the rare-earth ion with the individual spins in the host or the interactions within the spin bath. This paper presents a method to study the interactions and the resulting dynamics in detail. By doing this, we aim to improve the decoupling techniques

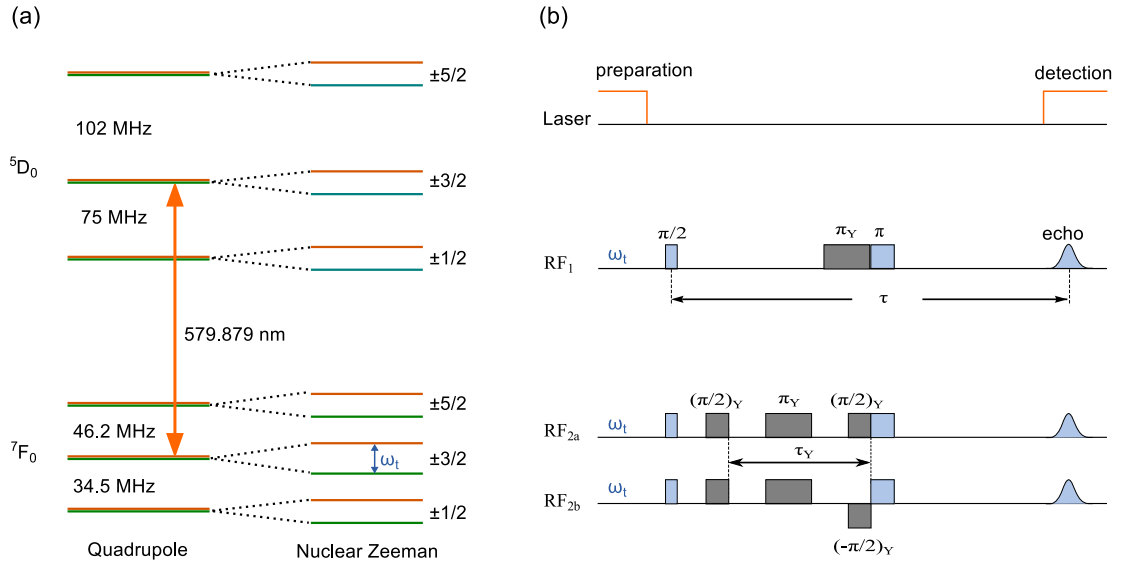

Figure 1. (a) Hyperfine energy level structure for Site 1 Eu^{3+} ions in $^{151}Eu^{3+}$: Y_2SiO_5 [24]. The transition used for ZEFOZ is indicated by ω_t. (b) Pulse sequences used in the experiments. The optical field is for preparing a population difference between the $+3/2$ and $-3/2$ states before applying RF pulses and optically detecting the spin echo signal. Sequence RF_1 is for measuring the spectrum of the Y^{3+} ions, their nutation frequency and their coupling strength with Eu^{3+} ion. Sequences RF_{2a} and RF_{2b} are for measuring the coherence time of the frozen-core Y^{3+} ions. In each pulse sequence, the blue-colored pulses are a two-pulse spin echo sequence of the Eu^{3+} while the gray used to drive the Y^{3+} spin transition.

and to investigate the possibility of using the host spins as a resource for conducting quantum computing operations.

The particular system investigated here is Eu^{3+}: Y_2SiO_5. In the previous study, when we demonstrated a hyperfine coherence time of six hours in this system [17], we also determined that the interactions between the Eu^{3+} and the nearby Y^{3+} spins are still the dominant decoherence source. Thus, while properties of bulk Y^{3+} spins in Y_2SiO_5 have been studied by Dupree *et al* [23], in this paper, techniques are developed to study the dynamics of these Y^{3+} spins in detail.

2. Theory

In Eu^{3+}: Y_2SiO_5, the Eu^{3+} ions can substitute the Y^{3+} ions in one of two sites of C_1 symmetry, which were referred to as Site 1 and Site 2 [24]. Each crystallographic site consists of a pair of magnetically inequivalent subsites, related by a rotation about the crystal's C_2 axis. For the current work, we studied the $^{151}Eu^{3+}$ ion in one of the two magnetic subsites of site 1, embedded in a bath consisting of Y^{3+} spins in both crystallographic sites.

The hyperfine structure of Eu^{3+}: Y_2SiO_5 is determined by several interactions and can be described by a reduced spin Hamiltonian for each electronic state [25, 26]:

$$H = \hat{\boldsymbol{I}} \cdot \boldsymbol{Q} \cdot \hat{\boldsymbol{I}} + \boldsymbol{B} \cdot \boldsymbol{M} \cdot \hat{\boldsymbol{I}} + (\boldsymbol{B} \cdot \boldsymbol{Z} \cdot \boldsymbol{B})\hat{\boldsymbol{E}}. \quad (1)$$

Here $\boldsymbol{B}$ is the external magnetic field, $\hat{\boldsymbol{I}}$ the nuclear spin operator, and $\hat{\boldsymbol{E}}$ the identity operator. The first term is the nuclear quadrupole interaction with $\boldsymbol{Q}$ the effective quadrupole tensor. This splits the $I = \frac{5}{2}$ electronic singlet states of Eu^{3+} into three doubly degenerate hyperfine states in zero field, with splittings of order 10 MHz. The second term is the nuclear Zeeman interaction, with $\boldsymbol{M}$ the effective Zeeman tensor, which is anisotropic in Eu^{3+}: Y_2SiO_5. The final term is the quadratic Zeeman interaction, with $\boldsymbol{Z}$ the quadratic Zeeman tensor. This term does not contribute to the hyperfine splitting, but it does contribute to the interaction between the Eu^{3+} and Y^{3+} ions. The energy level structure of site 1 Eu^{3+}: Y_2SiO_5 is shown in figure 1.

The six-hour coherence time in the previous work was observed on the Eu^{3+} ion's $m_I = -3/2 \leftrightarrow 3/2$ hyperfine transition by the application of the ZEFOZ and DDC techniques mentioned above [17]. The chosen ZEFOZ point occurs at a field magnitude of 1.29 T and is referred to here as the critical point $\mathbf{B}_{cp}$ to reflect the zero gradient in the Zeeman splitting. In addition to the zero gradient, the critical point field also induces a large magnetic moment ($\boldsymbol{Z} \cdot \boldsymbol{B}_{cp}$ from equation (1)). The local magnetic field generated by this moment, in turn, creates a frozen core of Y^{3+} ions whose frequencies are detuned from the bulk Y^{3+} ions. It is interactions with these frozen core Y^{3+} ions that dominate the Eu^{3+} ion hyperfine decoherence, because the reduced field sensitivity of the Eu^{3+} means its interactions with the more distant bulk spins are negligible. Thus, we will concentrate our study on the interactions between the Eu^{3+} ion and the frozen core Y^{3+} ions.

Depending on their spatial position relative to the Eu^{3+} ion, the spin properties for each frozen-core Y^{3+} ion, such as the detuned spin frequency, coherence time, or lifetime, can be different. Similarly, independently flipping a frozen-core Y^{3+} spin at different sites caused a unique frequency shift on the Eu^{3+} hyperfine transition. These properties are determined by the magnetic dipole–dipole interactions between the Eu^{3+} and Y^{3+} ions. Here, these interactions are treated as a perturbation on the reduced spin Hamiltonian of the Eu^{3+} ion [27], from which the magnetic dipole moment of the Eu^{3+} is determined.

First, the detuned resonant spin frequency of the ith frozen-core Y^{3+} spin is given by:

$$df_{Yi} = \gamma|\boldsymbol{B} + \boldsymbol{dB_i}| - \gamma|\boldsymbol{B}|, \tag{2}$$

where $\gamma = 2.09$ MHz T^{-1} is the gyromagnetic ratio of Y^{3+}, $\boldsymbol{B}$ is the applied magnetic field and $\boldsymbol{dB_i}$ is the additional field of the Eu^{3+} ion's magnetic moment at the position of the Y^{3+} ion:

$$\boldsymbol{dB_i} = \frac{\mu_0}{4\pi}\left(\frac{3(\boldsymbol{\mu}_{Eu}\cdot\boldsymbol{r}_i)\boldsymbol{r}_i}{|\boldsymbol{r}_i|^5} - \frac{\boldsymbol{\mu}_{Eu}}{|\boldsymbol{r}_i|^3}\right), \tag{3}$$

where μ_0 is the vacuum permeability, $\boldsymbol{r_i}$ is the displacement of the ith Y^{3+} ion relative to the Eu^{3+} ion and $\boldsymbol{\mu}_{Eu}$ is the magnetic moment of the Eu^{3+} spin.

From equation (1), $\boldsymbol{\mu}_{Eu}$ has two different contributions in the presence of an external magnetic field, which are the nuclear magnetic moment $(\boldsymbol{M}\cdot\hat{\boldsymbol{I}})$ and the induced moment $(\boldsymbol{Z}\cdot\boldsymbol{B}_{cp})$. The Eu^{3+} electronic ground state has a nuclear magnetic moment comparable to that of Y^{3+}, thus the frozen core effect is expected to be very small at zero field. However, the induced moment is linearly dependent on the applied field magnitude. At the applied critical-point field the induced moment, 150 MHz T^{-1}, is nearly two orders of magnitude larger than the nuclear magnetic moment, so the contribution to the frequency detuning from the nuclear magnetic moment can be ignored.

While the detuned spin frequency of the frozen-core Y^{3+} ions df_{Y_i} is dominated by the induced moment of the Eu^{3+} ion, the frequency shift of the Eu^{3+} hyperfine transition resulting from flipping a Y^{3+} spin is determined by the nuclear magnetic moment only. The spin flip of the ith frozen-core Y^{3+} ion produces a magnetic field perturbation $\boldsymbol{\delta B_i}$ at the Eu^{3+} site, given by:

$$\boldsymbol{\delta B_i} = \frac{\mu_0}{4\pi}\left(\frac{3(\boldsymbol{\mu}_{Y}\cdot\boldsymbol{r}_i)\boldsymbol{r}_i}{|\boldsymbol{r}_i|^5} - \frac{\boldsymbol{\mu}_{Y}}{|\boldsymbol{r}_i|^3}\right), \tag{4}$$

where $\boldsymbol{\mu}_Y$ is the magnetic moment of the Y^{3+} spin. This field perturbation results in a frequency shift of Eu^{3+} hyperfine transition given by:

$$\delta f_i = \boldsymbol{\Delta\mu}_{Eu}\cdot\boldsymbol{\delta B_i}, \tag{5}$$

where $\boldsymbol{\Delta\mu}_{Eu}$ is the difference in the Eu^{3+} magnetic moment between the hyperfine ground and excited states, which equals the transition's field sensitivity. Given that the quadratic Zeeman tensor $\boldsymbol{Z}$ has the same effect on all the hyperfine states [26], the induced moment is the same for all the hyperfine states, thus $\boldsymbol{\Delta\mu}_{Eu}$ is given by the difference in the nuclear magnetic moment of the two hyperfine states. At $\mathbf{B}_{cp}$, $\boldsymbol{\Delta\mu}_{Eu} = 0$, so flipping a Y^{3+} spin does not produce any frequency shift in the Eu^{3+} hyperfine transition. When the field is detuned from the critical point, there is a non-zero value of $\boldsymbol{\Delta\mu}_{Eu}$, quadratically dependent on the amount of field detuning from the critical point.

In the experiment, the Eu^{3+} frequency shift δf_i in equation (5) was measured using a spin echo technique as shown in the RF_1 pulse of figure 1. A resonant π pulse (π_Y) was applied to one Y^{3+} site to drive a Y^{3+} spin flip, and the effect on the coherence of the Eu^{3+} ion was measured using a standard echo sequence. In a two pulse spin echo measurement, a frequency shift during the echo sequence results in a phase shift in the echo signal. Thus, when a π_Y pulse is applied resonant with one of the frozen core Y^{3+} spin frequencies, a well-defined phase shift of the Eu^{3+} echo signal might be expected. However, this is only true when the Y^{3+} ensemble is initialized in the same state, whereas in our system the Y^{3+} ensemble is in a thermal state, with the two spin states equally populated. The effect of this pulse sequence for thermal ensembles is known from polarization transfer experiments in NMR [28]: the Eu^{3+} echo amplitude is modulated at a frequency δf_i. The echo amplitude as a function of the echo delay time τ can thus be written

$$E(\tau) = [1 + d_{mod}(e^{-\frac{\tau}{T_{1Y}}}\cos(2\pi\delta f_i\tau) - 1)]e^{-\frac{\tau}{T_2}}, \tag{6}$$

where T_2 is the Eu^{3+} coherence time and T_{1Y} is the lifetime of the Y^{3+} ion, which leads to decay of the modulation . d_{mod} describes the depth of the modulation. As we will show, the Y^{3+} Rabi frequency is similar to the Y^{3+} ion inhomogeneous broadening, so not all Y^{3+} ions see a π_Y pulse, reducing the depth of the modulation by about half. At a given field detuning from the critical point ($\boldsymbol{\Delta\mu}_{Eu}$ is fixed), each individual frozen-core Y^{3+} site corresponds to a unique echo modulation frequency. A measurement of the modulation can work out the interaction strength δf_i (equation (5)) between this Y^{3+} ion and the Eu^{3+} ion. We note that this modulation is different to that often observed in photon echo measurements due to exciting multiple sublevels with the optical

pulses (e.g. [29]), including due to superhyperfine coupling to nuclear spins [30, 31]. In that case, the optical pulses drive multiple transitions and the modulation, at the frequency of the coupled nuclear spin splitting, is due to the interference of these different excitations. In our experiments, the modulation is due to the interference of different Eu^{3+} ions in the ensemble, and occurs at the frequency of the Eu^{3+}–Y^{3+} interaction itself.

The modulation effect is only observable in a particular magnetic field regime: close to, but not exactly on, a critical point. In the above discussion, the focus was on one individual frozen-core Y^{3+} ion while the echo decay due to the reconfiguration of other Y^{3+} ions was ignored. This is only true when the measurement is performed near a critical point where the effect of the bulk Y^{3+} spin flips is negligible due to the small field sensitivity. Otherwise, if the field is completely away from a critical point, the echo signal decays quickly to zero due to the fast spin flips of the bulk Y^{3+} ions before a slow modulation caused by a frozen-core Y^{3+} ion can be observed. Equally, however, if there is a spontaneous spin flip of the frozen-core Y^{3+} spin during the modulation period $1/(\delta f)$, an echo modulation for an individual Y^{3+} ion produced by the π_Y pulse will not be observable, thus, the echo modulation period must be made sufficiently short. In order to shorten the modulation period $1/(\delta f)$ such that it is shorter than the lifetime of the frozen-core Y^{3+} spins, the field sensitivity needs to be increased by detuning the field from the critical point. Hence, the field alignment should be made such that:

$$\frac{1}{R_b} \ll \frac{1}{\delta f} < \frac{1}{R_f}, \tag{7}$$

where $1/R_b = 3.5$ ms is the correlation time of the bulk Y^{3+} ions [32] and $1/R_f$ is the correlation time of the frozen-core Y^{3+} spins. In the previous study, at the investigated critical point $\mathbf{B}_{cp}$, $1/R_f$ was measured to be 59 s [17].

3. Experiment

The experimental setup is described in [17] and will only be briefly outlined here. A 0.01% doped Eu^{3+}: Y_2SiO_5 crystal was maintained at 2 K in a bath cryostat that incorporates a superconducting magnet. The hyperfine transitions of the Eu^{3+} ion and the nuclear spin transition of the Y^{3+} ions were excited using a six turn coil with a diameter of 6 mm, driven by a 40 dBm RF source, which resulted in a Rabi frequency $\Omega_{RF} = 7.9$ kHz. Raman heterodyne detection [33] was used to observe the Eu^{3+} ion's spin coherence optically via the $^7F_0 \rightarrow {}^5D_0$ transition at 579.879 85 nm. A spectrum analyser was used to record the amplitude of the Raman heterodyne signal. The laser power incident on the crystal was 30 mW and was gated by an 80 MHz acoustic-optic modulator. Prior to applying each Raman heterodyne pulse sequence, the system was prepared with an optical re-pump and burn scheme such that the Eu^{3+} ensemble was initialized in the $+3/2$ state. The magnetic field was aligned to achieve the critical field configuration of the $3/2 \leftrightarrow -3/2$ transition occuring at $|\boldsymbol{B}_{cp}| = 1.29$ T. To satisfy equation (7), all the measurements to be discussed in this paper were performed at a field detuned by (1.6 ± 1) mT from this critical point.

4. Results

The measurement of the spectrum for these resonant spin frequencies was performed using the RF_1 pulse sequence in figure 1, scanning the frequency of the π_Y pulse and observing the change in the amplitude of the spin echo from the Eu^{3+} spins. The frequency of the π_Y pulse was scanned 9 kHz about the expected frequency of the bulk Y spins estimated from field applied (1.290 ± 0.001 T) and the gyromagnetic ratio of the Y^{3+} ion (2.09 MHz T^{-1}). The length of the π_Y pulse was set to 4.5 ms. The delay between the $\pi/2$ and π pulses applied to the Eu^{3+} spins was 2.6 s. The resulting spectrum is shown in figure 2. The expected resonant frequency of the of the 20 nearest Y^{3+} ions, calculated using equation (1), are shown in figure 2 (a). We see general agreement between theory and experiment, with one clearly resolved peak at 2.706 MHz and a series of poorly resolved peals down to 2.704 MHz. The extreme frequency peaks p_1 and p_5 in the spectrum are assigned as Y^{3+} sites Y_1 and Y_2 as shown in 2 (b). We do not expect to observe a peak at the resonant frequency of the bulk Y^{3+} spins as their interaction with the Eu^{3+} spins is expected to be weak and their lifetimes short compared to the timescale of the measurement, hence perturbing these spins is unlikely to significantly alter the evolution of the Eu^{3+} spins.

The amplitude of the contribution of each Y^{3+} site is determined by the coupling strength $\boldsymbol{\delta B_i}$ and the echo delay τ. The largest reduction in the echo amplitude corresponds to the peaks where the product of the coupling strength and the echo delay time is close to π. Hence, the peaks with the largest modulation depth (p_1 and p_5) may not necessarily have the strongest coupling strength.

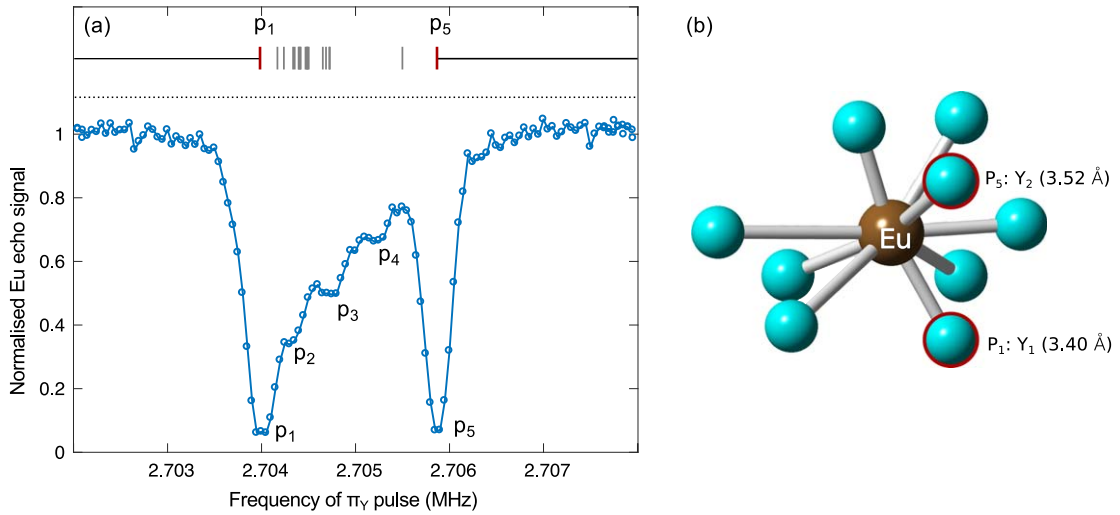

Figure 2. (a) The measured spectrum of the frozen-core Y^{3+} spin transitions near the critical point $\mathbf{B}_{cp}$, with the Eu^{3+} echo amplitude plotted against the frequency of the π_Y-pulse (bottom). Top, the calculated frequency of the spin transition for the nearest 20 frozen core-Y^{3+} ions. Each vertical line represents the frequency detuning for a Y^{3+} site. Red lines are those Y^{3+} sites which are assigned with the experimental peaks as marked. (b), Assignments of the resolved peaks p_1 and p_5 to sites around the Eu ion (circled in red).

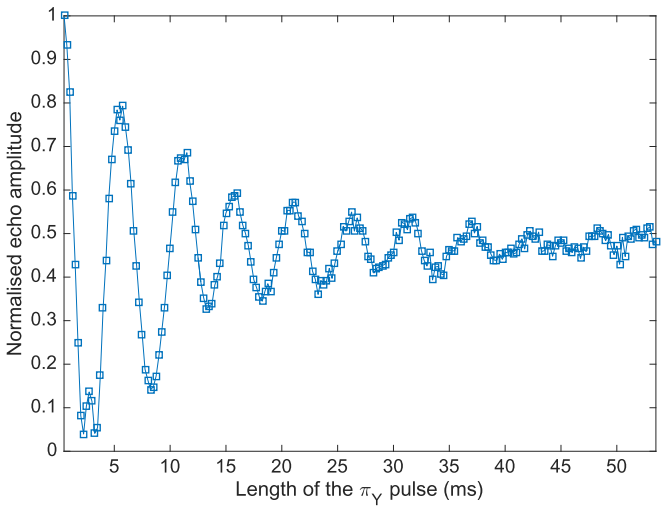

Figure 3. Nutation measurement of frozen core Y^{3+} site p_5, measured via the Eu^{3+} ion. The frequency of the nutation gives the Y^{3+} ion Rabi frequency of 191 Hz, and the decay can be attributed to inhomogeneity in the RF field across the sample.

The FWHM of peak p_5 was 360 Hz. This is dominated by two effects: the 200 Hz Fourier width of the π_Y pulse and the inhomogeneity in the applied magnetic field, which is on the order of 0.1 mT and causes approximately 200 Hz of inhomogeneous broadening of the Y^{3+} spins.

To optimize the π_Y pulse nutation measurements were conducted. This again used pulse sequence RF_1 in figure 1(b), this time with the frequency of the π_Y pulse set to be resonant with one of the Y^{3+} sites and with a fixed Eu delay τ. The Eu^{3+} echo amplitude was then observed while scanning the length of the π_Y pulse.

The measured nutation of peak p_5 is shown in figure 3, with the Eu^{3+} echo amplitude plotted against the length of the π_Y pulse. A clear nutation is observed with a Y^{3+} ion Rabi frequency of 191 Hz. There are multiple sources that can contribute to decay of the nutation, including inhomogeneous broadening of the Y^{3+} ions themselves, but in this measurement it is dominated by inhomogeneity in the applied RF field across the sample.

To determine the coherence time of the Y^{3+} spins, we performed a spin echo measurement on p_5 using the RF_{2a} and RF_{2b} sequences in figure 1(b). In both sequences, the single π_Y pulse is replaced with three pulses: $\pi/2$, π and $\pi/2$ for RF_{2a}, and $\pi/2$, π and $-\pi/2$ for RF_{2b}. The frequency of these pulses was set to be the resonant frequency of the p_5 site and the experiment was performed with a fixed Eu^{3+} delay τ of 1.8 s.

The purpose of these two sequences is as follows. If there is no decoherence over the Y delay time τ_Y, then the three pulses in RF_{2a} correspond to a $2\pi_Y$ pulse, that is, they return the Y^{3+} to its original state. The Eu^{3+} ion is

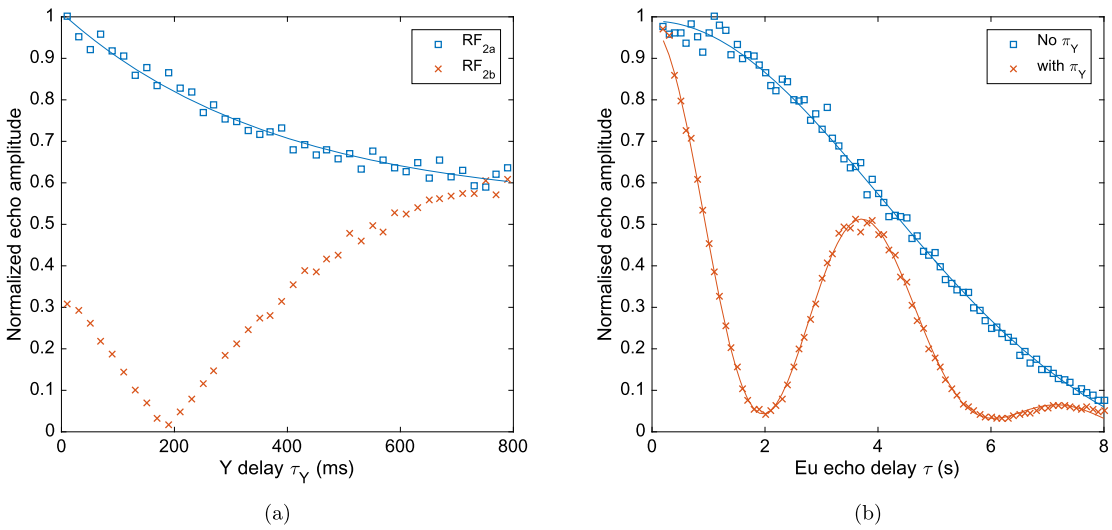

Figure 4. (a) Coherence time measurement of the frozen-core Y^{3+}via measurement of the Eu^{3+} ion's echo amplitude as a function of the Y^{3+} delay using two different pulse sequences, RF_{2a} (blue squares) and RF_{2b} (orange crosses). The solid blue line is a fit to the RF_{2a} data, which resulted in a coherence time of 600 ms. (b) Modulation of the Eu echo amplitude by the frozen core Y^{3+} spins. Blue squares are the decay when there is no perturbing π_Y pulse, with the blue line a fit using the Mims model (see text for details). Orange crosses are the modulation that appears when the π_Y pulse is on, with the fit given by equation (6).

unperturbed as long as τ_Y is short compared to the Eu delay τ. As τ_Y increases and the Y^{3+} ions decohere, the pulses are less effective at returning the ion to its original state, leading to increasing Eu^{3+} decoherence. Conversely, at short τ_Y the sequence RF_{2b} corresponds to a π_Y pulse, and which perturbs Eu^{3+} echo, but as τ_Y increases this effect is reduced as the Y^{3+} ions decohere. Ignoring inhomogeneity in the ions, the initial ($\tau_Y = 0$) echo amplitude for RF_{2a} is 1, but for RF_{2b} it is dependent on the Eu^{3+} delay time τ: $E_{RF_{2b}}(0) = \cos 2\pi\delta f_i \tau$.

The results of these two sequences are shown in figure 4(a) with the Eu^{3+} echo amplitude plotted against τ_Y. RF_{2b} produced an initial negative signal, which has been rectified by the spectrum analyzer, and shows a gradual rise in the signal with τ_Y. Likewise, sequence RF_{2a} shows the expected decay with increasing τ_Y, with a decay time constant of 400 ms. There are two components to this decay. The first is the exponential decay caused by decoherence of the Y^{3+} ions, as described above. The second component arises because the Y pulse sequence time is increasing, reaching up to 0.3 times the Eu^{3+} delay time. Since the Eu^{3+} dephasing is different during the Y^{3+} sequence time, the dephasing is not symmetric around the Eu^{3+} π pulse, and is not completely rephased. A fit to the RF_{2a} signal including these two contributions gave a Y^{3+} coherence time of 600 ms.

Finally, we measured the frequency shift δf on the Eu^{3+} ion caused by flipping a Y^{3+} ion by measuring the modulation of the Eu^{3+} echo (see equation (6)). We used sequence RF_1 with the frequency of the π_Y pulse set to peak p_5. Based on the nutation measurement, the length of the π_Y-pulse was set to be 2.75 ms. With this fixed π_Y pulse, the Eu^{3+} echo amplitude was recorded by varying the total Eu^{3+} delay τ. To observe the effect of the π_Y pulse on the Eu^{3+} echo decay, the Eu^{3+} echo amplitude with and without a π_Y-pulse were recorded sequentially for each delay.

The measured Eu^{3+} two pulse spin echo amplitude as a function of the total delay is shown in figure 4(b). In the absence of the π_Y pulse, the echo decays due to interactions with the bulk spin bath. The clear non-exponential decay is due to spectral diffusion, since the Y^{3+} spin bath is flipping on the timescale of the measurement. To account for this, the fit shown in figure 4(b) is to the empirical Mims model [34]:

$$E(\tau) = E_0 e^{-\left(\frac{\tau}{T_M}\right)^2}, \tag{8}$$

where T_m is the phase memory time. Adding the π_Y pulse causes a clear modulation, which was fit by equation (6) with the exponential T_2 decay term replaced with the Mims' fit from the unperturbed data. The fit gave a modulation frequency of $\delta f = 0.25$ Hz (the Eu^{3+}–Y^{3+} interaction strength), and a envelope decay rate of 14 ± 1 s (the Y^{3+} lifetime).

Previously, p_5 was assigned to site Y_2, so we can calculate the expected modulation frequency δf_{p5} in equation (5). At the experimental detuning from the critical field of 1.6 ± 1 mT, this gives an interaction strength of 0.5 ± 0.3 Hz. Given the large uncertainty, this is consistent with the measured value of 0.25 Hz. The measured lifetime value of 14 s, meanwhile, is consistent with the previously measured 59 s correlation time in the magnetic field perturbations acting on the Eu^{3+} ion $\mathbf{B}_{cp}$ [17], given that different Y^{3+} ions in the frozen core can be expected to have different lifetimes.

5. Discussion

We have demonstrated techniques to measure the transition frequency, homogeneous and inhomogeneous linewidths of the frozen core Y^{3+} spins surrounding the Eu^{3+} ion along with the interaction strength between the Eu^{3+} ion and the Y spins. The techniques can be refined, in particular by reducing the inhomogenuity in the applied DC and rf magnetic fields. With these improvements it should be possible to accurately characterize the Y^{3+} spin bath. Of particular interest will be to use this detailed knowledge to model the effect of the DDC control pulses used to extend coherence times in [17] on the dynamics of the bath.

The successful demonstrations of DDC in rare-earth ion systems operate in the regime where the system-bath interaction is sufficiently weak compared to the interactions within the bath that the effect of the control pulses on the bath dynamics can be neglected. In this regime, the action of the bath on the system can be treated as a classical field. Generic dynamic decoupling pulse sequences can be successfully employed without detailed knowledge of the structure of the bath or the coupling to it. Ultimately, however, the maximum coherence time that can be achieved using these generic sequences will be limited by this back action on the bath due to the residual system-bath coupling. A detailed model of the bath will allow the limit of the existing DDC sequences to be identified and provide the basis for developing new DDC sequences to minimize the effect of the back action.

Beyond providing information relevant to the dephasing mechanism of the europium Eu^{3+}, the current results also demonstrate the potential to use the Y^{3+} frozen core as a quantum resource suitable for quantum information processing, with a moderate number of qubits. The different Y^{3+} sites in the frozen core can be addressed via their spin transition frequency and the magnetic dipole–dipole coupling between the Y^{3+} and Eu^{3+} ions can be used to enact two qubit gates. The pulse sequences shown in figure 1(b), which we used to characterize the frozen core, are entangling gates between the Eu^{3+} and the Y^{3+} spin. The difference between our measurements and what is required for a quantum processing operation was that the Y^{3+} spins were not initialized. However, the Y^{3+} spins could be initialized by repeatedly initializing the Eu^{3+} spin through optical pumping and performing SWAP gates with each of the Y^{3+} spins in the frozen core.

The number of Y^{3+} spins that can be resolved and used as qubits depends both on the inhomogeneous broadening on the Y^{3+} spin transition and the strength of the interaction between the induced magnetic moment of the Eu^{3+} ion and the Y^{3+} spins. At the current ZEFOZ point this interaction is of the order of kilohertz, but since the moment is linear with field, critical points at higher magnetic fields will have larger interaction strengths. With critical points theoretically identified at fields of up to 7 T [27], potentially detunings in the frozen core of the order of 10 kHz could be realized. The observed inhomogeneous broadening was of the order of 350 Hz, which was consistent with the combination of the Fourier width of the excitation pulses chosen and the known inhomogeneity in the applied magnetic field. The latter source can be almost completely eliminated by shimming the applied magnetic field using standard techniques from high resolution NMR. If longer pulses are used, the residual broadening is likely to be dominated by the magnetic dipole–dipole coupling between the Y^{3+} spins. In particular, Y^{3+} ions in the frozen core but not initialized will contribute to the inhomogeneous broadening. The magnetic field caused by the randomly oriented spin bath has been estimated at 0.01 mT [13], and corresponds to an inhomogeneous broadening on the Y^{3+} ion of 20 Hz. If the inhomogeneity in the applied field can be reduced to this level, seven of the nearest ten Y^{3+} spins, for example, would be resolvable. The other three spins either have very small frequency shifts (Y_6, Y_{10}) or a frequency coincident with another Y^{3+} site (Y_4).

Once the Y^{3+} spins can be initialized, the number of gate operations that can be performed depends both on the coherence time of the frozen core Y^{3+} spins and on the interaction strength between the nuclear magnetic moment of the Eu^{3+} and the magnetic moment of the Y^{3+} spins. The coherence time of the p_5 Y^{3+} spin of 600 ms and the 0.25 Hz interaction strength currently limits the system to only a few gate operations, at most, between the Eu^{3+} and Y^{3+} spins. It is possible to increase the interaction with the Eu^{3+} spin by moving further away from the ZEFOZ point, but moving away from ZEFOZ will come at the expense of decreasing the coherence time of the Eu^{3+} hyperfine transition. Another method to increase the number of gate operations is to operate at ZEFOZ points at higher applied magnetic fields and hence increase the extent of the frozen core. This has the potential to not only increase the number of spins resolved, as discussed above, but also to significantly increase the coherence times of both the Eu^{3+} hyperfine transitions and the neighboring Y^{3+} spins. Further extension of the frozen core in Y_2SiO_5 could be obtained by replacing the Eu^{3+} with a Kramers ion such as Er^{3+}, which has a magnetic moments three orders of magnitude greater that the moment induced on the Eu^{3+} ion in the current work. [18].

Quantum operations can be performed on this ensemble-based spin frozen core system in a way similar to liquid-state NMR[35]. However, in the current system, the Y^{3+} nuclear spins can be manipulated optically, via their interaction with the Eu^{3+} ion. This has two key advantages. First, unlike in NMR the spins can be initialized via optical pumping of the Eu as described above. Second, photonic quantum information can be transferred

onto the nuclear spins of the frozen core, where it can be stored or processed. This ability could be used, for example, to extend the functionality of quantum memories.

6. Conclusion

We have demonstrated techniques to characterize the properties of host spins in the frozen core surrounding optically active rare-earth ions. In the case of the system investigated, Eu^{3+}: Y_2SiO_5, the lifetime and coherence time of the frozen core Y^{3+} spins was found to be long enough to potentially allow the use of SWAP gates with the Eu^{3+} to initialize the Y^{3+} spins. We have discussed how the coherence time and spectral resolution of the spins could be increased by increasing the extent of the frozen core, potentially enabling the use of the spin frozen core as a resource for quantum processing operations.

Acknowledgments

This work was supported by the Australian Research Council Centre of Excellence for Quantum Computation and Communication Technology (Grant No. CE110001027). MZ is supported by the Science, Technology and Innovation Commission of Shenzhen Municipality (No. ZDSYS20170303165926217, No. JCYJ20170412152620376)) and Guangdong Innovative and Entrepreneurial Research Team Program (Grant No. 2016ZT06D348). RLA is a recipient of an Australian Research Council Discovery Early Career Researcher Award (project No. DE170100099).

References

[1] Hedges M P, Longdell J J, Li Y and Sellars M J 2010 *Nature* **465** 1052
[2] Sabooni M, Li Q, Kröll S and Rippe L 2013 *Phys. Rev. Lett.* **110** 133604
[3] Jobez P, Usmani I, Timoney N, Laplane C, Gisin N and Afzelius M 2014 *New J. Phys.* **16** 083005
[4] Lovrić M, Suter D, Ferrier A and Goldner P 2013 *Phys. Rev. Lett.* **111** 020503
[5] Heinze G, Hubrich C and Halfmann T 2013 *Phys. Rev. Lett.* **111** 033601
[6] Laplane C, Jobez P, Etesse J, Gisin N and Afzelius M 2017 *Phys. Rev. Lett.* **118** 210501
[7] Ferguson K R, Beavan S E, Longdell J J and Sellars M J 2016 *Phys. Rev. Lett.* **117** 020501
[8] Laplane C, Jobez P, Etesse J, Timoney N, Gisin N and Afzelius M 2015 *New J. Phys.* **18** 013006
[9] Clausen C, Usmani I, Bussieres F, Sangouard N, Afzelius M, de Riedmatten H and Gisin N 2011 *Nature* **469** 508
[10] Saglamyurek E, Sinclair N, Jin J, Slater J A, Oblak D, Bussieres F, George M, Ricken R, Sohler W and Tittel W 2011 *Nature* **469** 512
[11] Equall R W, Sun Y, Cone R and Macfarlane R 1994 *Phys. Rev. Lett.* **72** 2179
[12] Könz F, Sun Y, Thiel C, Cone R, Equall R, Hutcheson R and Macfarlane R 2003 *Phys. Rev.* B **68** 085109
[13] Fraval E, Sellars M and Longdell J 2004 *Phys. Rev. Lett.* **92** 077601
[14] Fraval E, Sellars M and Longdell J 2005 *Phys. Rev. Lett.* **95** 030506
[15] Thiel C, Böttger T and Cone R 2011 *J. Lumin.* **131** 353
[16] Böttger T, Thiel C, Cone R and Sun Y 2009 *Phys. Rev.* B **79** 115104
[17] Zhong M, Hedges M P, Ahlefeldt R L, Bartholomew J G, Beavan S E, Wittig S M, Longdell J J and Sellars M J 2015 *Nature* **517** 177
[18] Rančić M, Hedges M P, Ahlefeldt R L and Sellars M J 2018 *Nat. Phys.* **14** 50
[19] Ortu A, Tiranov A, Welinski S, Fröwis F, Gisin N, Ferrier A, Goldner P and Afzelius M 2018 *Nat. Mater.* **17** 671
[20] Schraft D, Hain M, Lorenz N and Halfmann T 2016 *Phys. Rev. Lett.* **116** 073602
[21] Viola L and Lloyd S 1998 *Phys. Rev.* A **58** 2733
[22] Viola L, Knill E and Lloyd S 1999 *Phys. Rev. Lett.* **82** 2417
[23] Dupree R and Smith M 1988 *Chem. Phys. Lett.* **148** 41
[24] Yano R, Mitsunaga M and Uesugi N 1991 *Opt. Lett.* **16** 1884
[25] Teplov M 1968 *Sov. Phys. JETP* **26** 872
[26] Macfarlane R M and Shelby R M 1987 Coherent transient and holeburning spectroscopy of rare earth ions in solids *Spectroscopy of Solids Containing Rare Earth Ions* ed A A Kaplyanskii and R M Macfarlane (Amsterdam: North-Holland)
[27] Longdell J, Alexander A and Sellars M 2006 *Phys. Rev.* B **74** 195101
[28] Morris G A and Freeman R 1979 *J. Am. Chem. Soc.* **101** 760
[29] Mitsunaga M, Yano R and Uesugi N 1992 *Phys. Rev.* B **45** 12760
[30] Lambert L Q 1973 *Phys. Rev.* B **7** 1834
[31] Car B, Veissier L, Louchet-Chauvet A, Le Gouët J-L and Chanelière T 2018 *Phys. Rev. Lett.* **120** 197401
[32] Arcangeli A, Lovrić M, Tumino B, Ferrier A and Goldner P 2014 *Phys. Rev.* B **89** 184305
[33] Mlynek J, Wong N, DeVoe R, Kintzer E and Brewer R 1983 *Phys. Rev. Lett.* **50** 993
[34] Mims W 1968 *Phys. Rev.* **168** 370
[35] Cory D G, Fahmy A F and Havel T F 1997 *Proc. Natl Acad. Sci. USA* **94** 1634